Continental Shelf Research 30 (2010) 575–587

Contents lists available at ScienceDirect

Continental Shelf Research

journal homepage: www.elsevier.com/locate/csr

18.6-year lunar nodal tides from altimeter data

Josef Y. Cherniawsky [a,*], Michael G.G. Foreman [a], Sok Kuh Kang [b], Remko Scharroo [c], A. Jane Eert [a]

[a] Institute of Ocean Sciences, Fisheries and Oceans Canada, P.O. Box 6000, Sidney, B.C., Canada V8L 4B2
[b] Korea Ocean Research and Development Institute, Seoul, Republic of Korea
[c] NOAA, Laboratory for Satellite Altimetry, Silver Spring, MD, USA

ARTICLE INFO

Article history:
Received 12 February 2009
Received in revised form
11 September 2009
Accepted 1 October 2009

Topical issue on " Tides in Marginal Seas" (in memory of Professor Alexei V. Nekrasov). The issue is published with support of the North Pacific Marine Science Organization (PICES).
Available online 31 October 2009

Keywords:
Satellite altimetry
Nodal tides
Harmonic analysis

ABSTRACT

Harmonic analyses of 16-year long time series of collocated TOPEX, Poseidon and Jason-1 altimeter data were carried out in the Pacific and western Atlantic Oceans and their marginal seas. These time series are sufficiently long to adequately separate the 18.6-year nodal satellites Q_{1n}, O_{1n}, K_{1n}, M_{2n} and K_{2n} from their parent constituents Q_1, O_1, K_1, M_2 and K_2. Editing criteria were used to eliminate results in areas where these satellites are weak (i.e., smaller than their formal error estimates), or where they are strongly affected by aliased low-frequency signals (e.g. in the Kuroshio, in the Gulfstream and in their extension regions). As expected from tidal theory, the phases of the altimetry-derived nodal satellites agree reasonably well with the phases of their parents. However, due to their relatively small amplitudes and the remaining influence from low-frequency aliased signals, the altimeter observed amplitude ratios between the nodal satellites and their parent constituents tend to exceed the values predicted by the theory.

Examination of diurnal and semidiurnal nodal amplitudes in select coastal areas and marginal seas around the Pacific and the western Atlantic Ocean allowed the assignment of a *nodal character* to regions, which were each classified as *nodal diurnal*, *nodal semidiurnal*, or *nodal mixed*, based on the nodal amplitudes in each band. While the areas with predominant diurnal tides are all *nodal diurnal*, the small nodal ratio of 0.037 for M_{2n} resulted in some regions with strong M_2 tides being classified as *nodal diurnal* or *nodal mixed*. The amplitude ratio between K_{2n} and K_2 is 0.30, making the K_{2n} amplitudes sometimes comparable to those of M_{2n}. However, this effect was not sufficient to make all the areas with dominant M_2 to be dominant *nodal semidiurnal*.

The observed amplitudes of the 18.6-year nodal constituent M_n are relatively small, 1.5–3.5 cm. These values significantly exceed its theoretical amplitudes, which are less than 1 cm almost everywhere. The analysed signals at M_n frequency are therefore of mostly non-tidal origin, part of the broad-band decadal ocean variability.

1. Introduction

The launch of the TOPEX/Poseidon satellite in 1992 with accurate radar altimeters has provided a new and very important data set for tidal analysis of global sea levels (e.g., Schrama and Ray, 1994; Ray, 1998; Cherniawsky et al., 2001) and resulted in very significant improvements in the accuracy of tidal prediction and of numerical tidal models (e.g., Egbert et al., 1994; Le Provost et al., 1998; Ray, 1999; Egbert and Erofeeva, 2002; Foreman et al., 2000, 2006). In 2002, the TOPEX/Poseidon satellite was replaced in the same orbit by Jason-1, also with a very accurate altimeter, thus extending the along-track time series of sea level observations to more than 16 years. The longer time series not only increases the accuracy of computed constituents but also allows analyses of minor constituents with frequencies relatively close to the major ones.

Modern harmonic analyses of tidal heights (Godin, 1972; Foreman, 1977, hereafter F77) follow the development of tidal potential theory by Doodson (1921) and express each constituent frequency as a linear superposition of six astronomical forcing harmonics, $\omega_k = l_1\tau + l_2 s + l_3 h + l_4 p + l_5 n' + l_6 p'$, where l_i are integers and τ, s, h, p, $-n'$ and p' are the mean rates of change of lunar time (with a mean period of 24.84 h) and of the longitudes of the moon (27.3 days), the sun (365.24 days), the lunar perigee (8.85 years), the moon's ascending node (18.61 years) and the solar perigee (20 392 years), respectively.

Usually when time series are limited to a few years, only the frequencies that differ by at least one multiple of the third harmonic (h) can be included in the analyses, provided that their expected amplitudes exceed background noise at the same frequency. But for longer time series, with durations approaching

* Corresponding author.
E-mail address:
josef.cherniawsky@dfo-mpo.gc.ca (J.Y. Cherniawsky).

0278-4343/$ - see front matter Crown Copyright © 2009 Published by Elsevier Ltd. All rights reserved.
doi:10.1016/j.csr.2009.10.002

or exceeding the 18.61-year nodal period, it is also possible to calculate the amplitudes and phases of nodal satellites of major constituents, which were previously included as part of the nodal corrections (Godin, 1972, 1986). The 18.6-year nodal variations have a direct effect on annual means of high water, low water and tidal range at the coast (e.g., Kaye and Stuckey, 1973; Amin, 1993), thus requiring detailed analyses of long-term sea level records.

One of the earliest analyses of nodal constituents was provided by Doodson (1924), who examined 19-year long variations in amplitudes of M_2 and N_2 in tidal records from Saint John, New Brunswick, and Bombay, India. His results for M_2 at Saint John showed a reasonably regular 19-year cycle, as expected from the nodal modulation. However variations in N_2 showed a more complex behaviour, likely due to the 9-year cycle in the longitude of lunar perigee. More recently, Amin (1985) analysed an 18.61-year long time series of sea level at stations on the west coast of Great Britain. His analyses of the 1963–1981 time series at Liverpool and Newlyn showed good agreement with theoretical nodal amplitude ratios for the major constituents, though the 0.032 ratio obtained for M_2 at Liverpool was smaller than the theoretical value of 0.037.

Another example of analyses of two 19-year long time series (1939–1957, 1958–1976) of hourly sea level in Victoria Harbour was described by Foreman and Neufeld (1991), who included more than 500 astronomical and shallow water constituents, of which about 180 (including 20 low-frequency and 47 shallow-water) constituents were found to be strong enough to be listed in the paper. In general, the observed nodal satellite ratios at Victoria agreed well with the tidal equilibrium values, though the ratios for nodal satellites of N_2 and M_2 were somewhat smaller, 0.028 and 0.034, than the 0.037 value predicted by the theory. These results demonstrate that, provided a tidal constituent amplitude lies above the noise level, its relative amplitude and phase generally agree with tidal potential theory predictions, thus confirming the usefulness of satellite correction algorithms employed by Godin (1972, 1986) and F77. However, local effects, such as friction in shallow water, or tidal resonance, also affect the observed nodal ratios, thus making them different from their astronomical values (e.g., Ku et al., 1985).

The 18.6-year constituent M_n was also included in the Foreman and Neufeld (1991) analyses and appears to be nonstationary. Its amplitudes for the two 19-year periods were 1.2 and 1.4 cm, respectively, which are about twice as high as the equilibrium value of 0.6 cm for this latitude (e.g., Pugh, 1987). The computed M_n phase values were also different for the two periods, 269° and 200°, respectively, i.e. 91° and 160° ahead of the M_n equilibrium phase. However, when using all data from the combined period of 1939–1976, the analysed M_n amplitude is somewhat smaller, 1.1 cm, and its phase of 300° is closer to the equilibrium phase. It is then natural to assume that for sufficiently long sea level timeseries, the analysed M_n amplitude and phase may be close to their equilibrium values. Such a result was indeed presented by Trupin and Wahr (1990), who used yearly averages of global tide gauge measurements from 260 stations with at least 19 years of data to show that the 18.6-year peak in the amplitude spectrum of "stacked" data (see Trupin and Wahr, 1990 for an explanation of "stacking") fits well the equilibrium spectral peak for M_n.

The 18.6-year modulation of diurnal and semidiurnal tides is of special interest because in many parts of the ocean it exerts a strong effect on tidal currents and vertical mixing. For example, Loder and Garrett (1978) and Garrett (1979) considered a simple model of vertical mixing on the shelf and found that even small, of the order of ε, variation in tidal currents can have a very noticeable effect on sea surface temperature (SST), $\delta T \sim (4\varepsilon/3)\Delta T$, where ΔT is the top to bottom temperature difference. The Loder and Garrett (1978) analyses of coastal SSTs on the east and west coasts of North America yielded amplitudes of the 18.6-year signal between 0.16 and 0.64 °C and phases in agreement with their model predictions.

Royer (1993) analysed ocean and air temperatures in the Gulf of Alaska and found that up to 30% of their low-frequency variations can be accounted for with the 18.6-year nodal signal. The long-term variations in tidal mixing and ocean temperatures can have important consequences for biological productivity and fisheries (e.g., Parker et al., 1995). Munk et al. (2002) discuss the role of such variations in tidal mixing, which include nodal modulations, on the oceanic poleward heat transport and climate. Ray (2007) extended the Loder and Garrett (1978) calculations of coastal SSTs and also provided a detailed analysis of the various hypotheses and mechanisms linking the nodal tides to decadal ocean variability. He concluded that the most likely process responsible for this variability is the 18.6-year modulation of diurnal tidal currents and vertical mixing.

Osafune and Yasuda (2006) found the bidecadal oscillations in the northwestern Pacific Ocean to be synchronized with the 18.6-year nodal cycle, while Yasuda et al. (2006) linked this cycle to Pacific Ocean climate variability and to the Pacific Decadal Oscillation (PDO). Hasumi et al. (2008) used a coupled ocean-atmosphere climate model to show that the 18.6-year cycle in tidal mixing around the Kuril Islands leads to coastal trapped waves propagating along the perimeter of the ocean, leading to 18.6-year periodicity in the Pacific Ocean variability. McKinnell and Crawford (2007) have found the nodal variations in northeast Pacific Ocean temperatures to be linked with the Pacific—North America (PNA) index, with the latter lagging the nodal signal by about 2 years. Nodal modulations also affect high latitude oceans temperatures and salinities (Yndestad et al., 2008) and the Arctic Ocean climate (Yndestad, 2006).

The effects of nodal tides on mixing can be readily investigated in numerical tidal models. For example, Foreman et al. (2006) found the nodal modulation to cause basin-wide variations of approximately 19% in the Bering Sea tidal energy flux, with even stronger variations in the straits of the Aleutian Islands, such as Seguam Pass, and around capes. It is therefore of interest to identify other areas where nodal modulation of diurnal or semidiurnal tides can have significant effects on ocean mixing and circulation, while examining the accepted wisdom that such effects are mainly due to diurnal tides.

In this paper, we carry out harmonic analyses of more than 16-year long records of TOPEX/Poseidon and Jason-1 (TPJ) along-track altimetry data in the Pacific and the western Atlantic Oceans (20S to 66N, 100E to 40W) in order to compute the nodal satellites of five major tidal constituents Q_1, O_1, K_1, M_2 and K_2. While these analyses are performed over the complete area, our attention is further focused on fifteen select regions, which include certain coastal areas and marginal seas. Some of these regions exhibit strong diurnal tides, while others show semi-diurnal or mixed tides. In the next two sections, we describe in some detail the processing and harmonic analysis procedures, with specific attention given to possible aliasing due the 9.916-day TPJ repeat period. The analyses results and spatial variations in nodal amplitudes and phases are presented and mean nodal ratios from altimetry are compared to the theoretical values. This comparison is carried out for the complete area and for each of the 15 regions.

2. Selection and preprocessing of altimeter data

Along-track altimetry data were extracted for the area of study using the Institute of Ocean Sciences (Sidney, BC) mirror of the Radar Altimetry Data System (RADS: http://rads.tudelft.nl/rads/rads.shtml) and associated software (Schrama et al., 2000; Naeije

et al., 2002; Scharroo, 2008). These data include 364 cycles (September 23, 1992–August 11, 2002) from TOPEX and Poseidon along their original ground tracks and 260 cycles (January 16, 2002–February 5, 2009) from Jason-1 altimeter, along the same ground tracks, thus giving a total of 624 cycles in the combined (TPJ) data set. However, during the tandem phase in 2002, the TOPEX/Poseidon satellite was in the same orbit and just 71 s behind Jason-1, so that the number of independent cycles is 603.

The default RADS geophysical corrections and flag selection (Scharroo, 2008) were used for each altimeter, except we retained the ocean tides in the data and used load tides derived from a current version of the GOT tidal model (GOT4.7), described in Ray (1999). We also ignored the somewhat conservative "radiometer land flag", thus allowing inclusion of data closer to land, while relying on other flags and editing to screen questionable data. RADS default parameters include reference frame offsets, ensuring that the three data sets are related at each location to the same reference level. Appendix A describes the editing and collocation of along-track data for each altimeter. Collocated data from each of the three altimeters were spliced together in chronological order, forming TPJ time series that are about 16.3 years long (September 23, 1992–February 5, 2009).

3. Harmonic analysis and aliasing

We calculate select tidal constants at each along-track TPJ location using the well known harmonic analysis procedure (F77), subsequently modified for TOPEX/Poseidon data (Cherniawsky et al., 2001, hereafter CFCH). As the time period and the number of observations (cycles) increase, it becomes possible to include in the analysis a larger number of constituents and satellites.

After several tests, we selected 36 constituents (including Z_0), based on relative amplitudes from tidal potential theory (Doodson, 1921; Godin, 1972; Pugh, 1987; F77; Foreman and Neufeld, 1991) and a posteriori plots of amplitudes in the area of study. These constituents are listed in Table 1 with their six Doodson (1921) numbers, frequencies, and the main (lowest-frequency) periods T_{al} of aliased signals due to the TPJ repeat period of 9.916 days (Parke et al., 1987; Ray, 1998, CFCH). The more than 16-year ($\sim$5970 days) long time series are long enough to allow good separation of potentially aliased pairs, such as $S_{sa}-K_1$ and P_1-K_2, but still somewhat too short to fully resolve the 18.6-year nodal satellites, denoted in Table 1 with a subscript n.

Examination of along-track error covariance matrices (Appendix B) shows only minor contributions from off-diagonal elements to constituent amplitude errors, even for the 18.6-year satellites. Mean values of error estimates σ_a ($=\sigma_k$ in Appendix B) are also listed in Table 1, together with the number of remaining valid locations N_v after the editing (explained below). However, these estimates do not (and cannot) include contributions from low-frequency aliased signals that are not in the analysis (e.g., Munk and Cartwright, 1966; Ray, 1998). For the frequency range in question, the oceanic sea level power spectrum is red. Therefore, analysed constituents with longer aliased periods T_{al} (Table 1) are expected to have larger errors due to such aliasing. In particular, K_1 ($T_{al}=173.3$ days) and K_{1n} (177.9 days) tend to show short-scale along-track amplitude variations that exceed their formal error estimates, which may be, at least in part, due to such low-frequency aliasing.

To minimize the effects of aliasing and of strong non-tidal signals, we adopted the following edit criteria when plotting, or tabulating computed amplitudes A and Greenwich phase lags G of the analysed constituents.

Table 1
Tidal constituents selected for harmonic analysis, listed in order of frequency, with Doodson numbers and main (lowest-frequency) alias periods T_{al}.

	Doodson numbers	Frequency (h^{-1})	T_{al} (day)	$\overline{A_a}$ (cm)	$\overline{\sigma_a}$ (cm)	N_v
Z_0	0 0 0 0 0 0	0.000000000	9.916	4.0	0.4	180350
M_n	0 0 0 0 1 0	0.000006129	9.930	**2.5**	0.8	138964
S_a	0 0 1 0 0-1	0.000114074	10.192	4.9	0.8	181567
S_{sa}	0 0 2 0 0 0	0.000228159	10.485	1.9	0.8	135022
M_m	0 1 0-1 0 0	0.001512152	15.490	0.9	0.6	73028
M_{sf}	0 2-2 0 0 0	0.002821933	30.189	0.9	0.7	11623
M_f	0 2 0 0 0 0	0.003050092	36.168	1.3	0.7	125292
σ_1	1-3 2 0 0 0	0.035908722	21.812	0.9	0.7	26024
Q_{1n}	1-2 0 1-1 0	0.037212374	68.682	**1.1**	0.8	39248
Q_1	1-2 0 1 0 0	0.037218503	69.383	**2.8**	0.9	124510
ρ_1	1-2 2-1 0 0	0.037420874	104.648	1.1	0.7	47120
O_{1n}	1-1 0 0-1 0	0.038724526	46.015	**2.7**	0.8	135078
O_1	1-1 0 0 0 0	0.038730654	45.706	**11.5**	0.8	185521
NO_1	1 0 0 1 0 0	0.040268594	23.775	1.3	0.6	84593
π_1	1 1-3 0 0 1	0.041438513	71.514	1.0	0.7	21505
P_1	1 1-2 0 0 0	0.041552587	88.925	6.1	0.9	153371
S_1	1 1-1 0 0 1	0.041666672	117.545	1.8	1.1	36958
K_1	1 1 0 0 0 0	0.041780746	173.322	**17.8**	0.9	177027
K_{1n}	1 1 0 0 1 0	0.041786875	177.856	**3.3**	0.8	97998
J_1	1 2 0-1 0 0	0.043292898	32.763	1.4	0.7	90542
$2N_2$	2-2 0 2 0 0	0.077487097	22.534	1.4	0.7	114749
μ_2	2-2 2 0 0 0	0.077689468	20.311	1.6	0.7	124293
N_2	2-1 0 1 0 0	0.078999249	49.548	8.2	0.8	186348
ν_2	2-1 2-1 0 0	0.079201620	65.251	2.0	0.8	123636
M_{2n}	2 0 0 0-1 0	0.080505272	62.648	**1.9**	0.8	114094
M_2	2 0 0 0 0 0	0.080511401	62.076	**37.9**	0.9	190562
λ_2	2 1-2 1 0 0	0.081821182	21.033	1.0	0.7	18709
L_2	2 1 0-1 0 0	0.082023553	20.640	1.4	0.7	101384
T_2	2 2-3 0 0 1	0.083219259	50.626	1.3	0.7	94039
S_2	2 2-2 0 0 0	0.083333333	58.772	13.8	0.9	185009
K_2	2 2 0 0 0 0	0.083561492	86.661	**4.2**	0.9	165825
K_{2n}	2 2 0 0 1 0	0.083567624	87.780	**1.7**	0.8	107801
η_2	2 3 0-1 0 0	0.085073644	40.400	0.8	0.6	25892
MO_3	3-1 0 0 0 0	0.119242055	26.324	1.0	0.8	7682
M_3	3 0 0 0 0 0	0.120767101	38.079	0.8	0.6	25407
M_4	4 0 0 0 0 0	0.161022801	31.038	1.2	0.8	16376

Mean amplitudes $\overline{A_a}$ from harmonic analysis and their mean error estimates $\overline{\sigma_a}$ are also shown, computed from data at N_v valid locations after applying the three editing criteria. Amplitude values marked in bold are for the constituents that are the subject of this work.

1. We require the analysed amplitudes to be larger than their error estimates: $A>\sigma$.
2. We require the computed complex amplitudes $C=A\exp(iG)$ on ascending and descending passes to agree near pass crossovers. Using $r=2|C_{asc}-C_{desc}|/|C_{asc}+C_{desc}|$, where C_{asc} and C_{desc} are average complex amplitudes at two ascending and two descending along-track locations near a crossover (Fig. A1), we exclude constituents near a crossover, and up to half the distance between the crossovers, when $r>0.5$.
3. We exclude locations where the root-mean-square sea level variability of the residual signal after detiding exceeds 1.6 m.

These edit criteria remove most, though not all suspect data. The number of remaining valid data locations (N_v in Table 1) depends on the relative amplitudes and susceptibility to aliasing of each constituent. For consistency, the last three columns in Table 1 were produced using all three edit criteria. However, we only used the first criterion when plotting amplitudes and phases of the three strongest constituents O_1, K_1 and M_2.

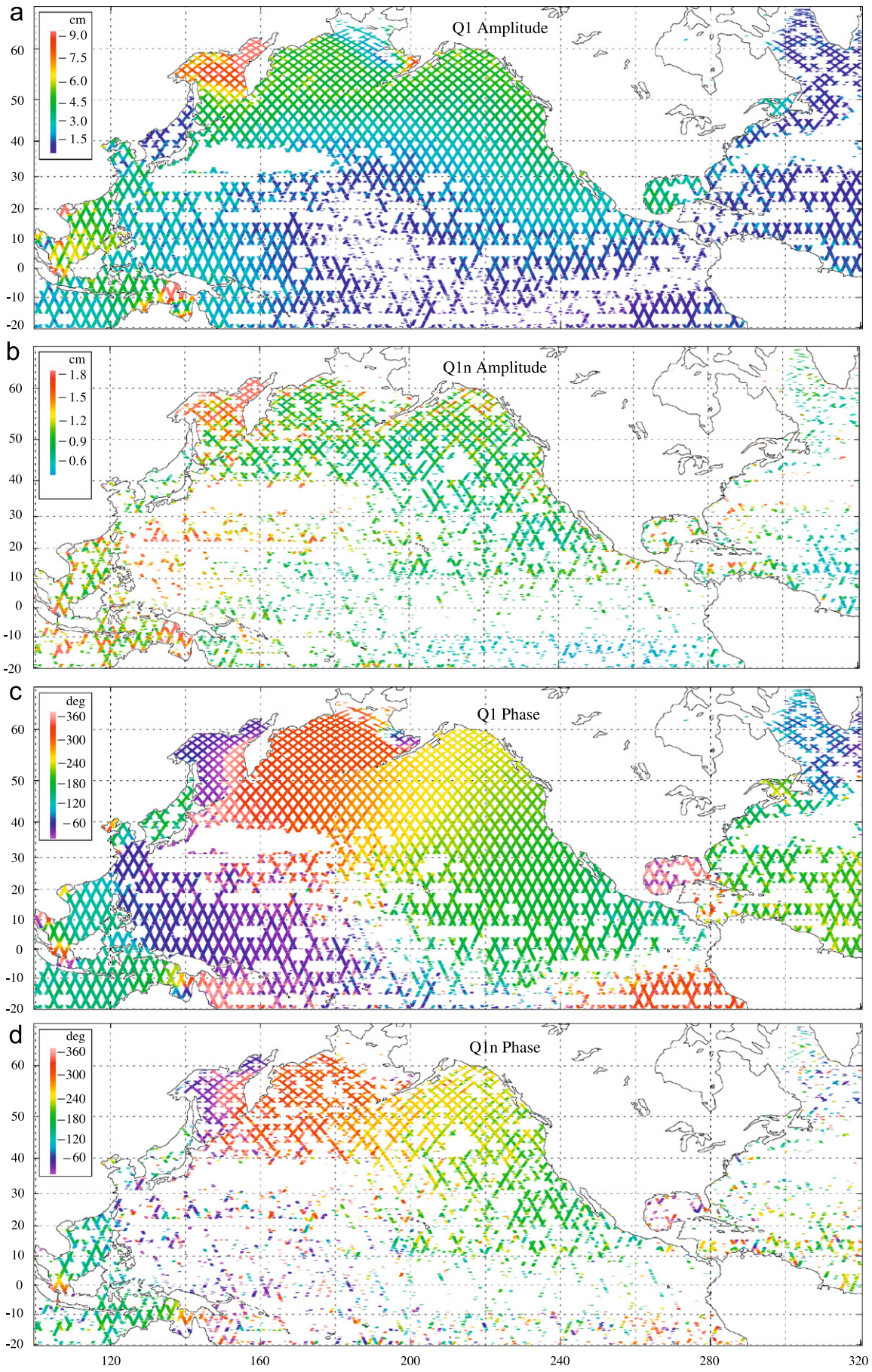

Fig. 1. Computed (a,b) amplitudes and (c,d) phases of (a,c) Q_1 and (b,d) Q_{1n}.

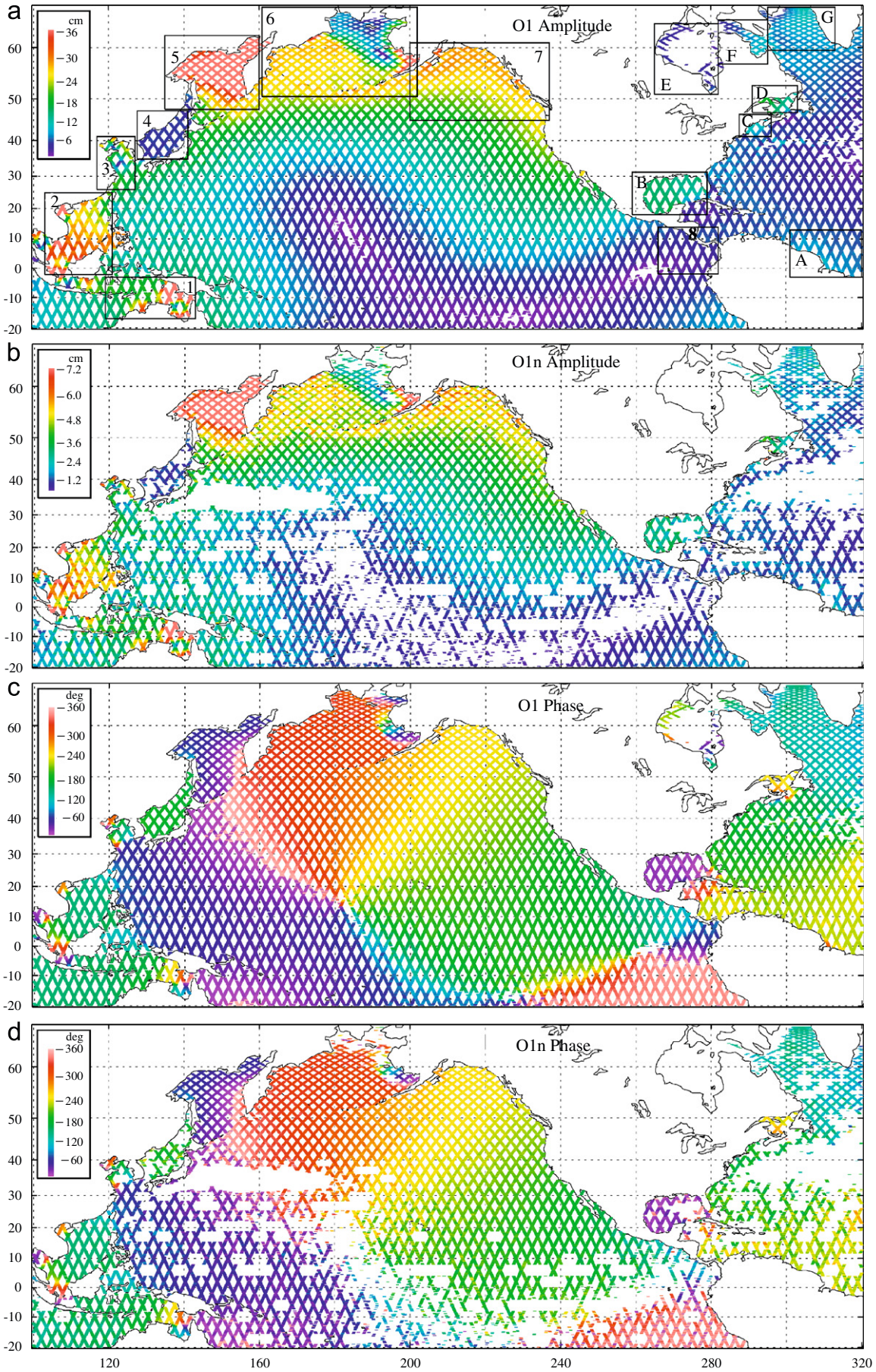

Fig. 2. Computed (a,b) amplitudes and (c,d) phases of (a,c) O_1 and (b,d) O_{1n}.

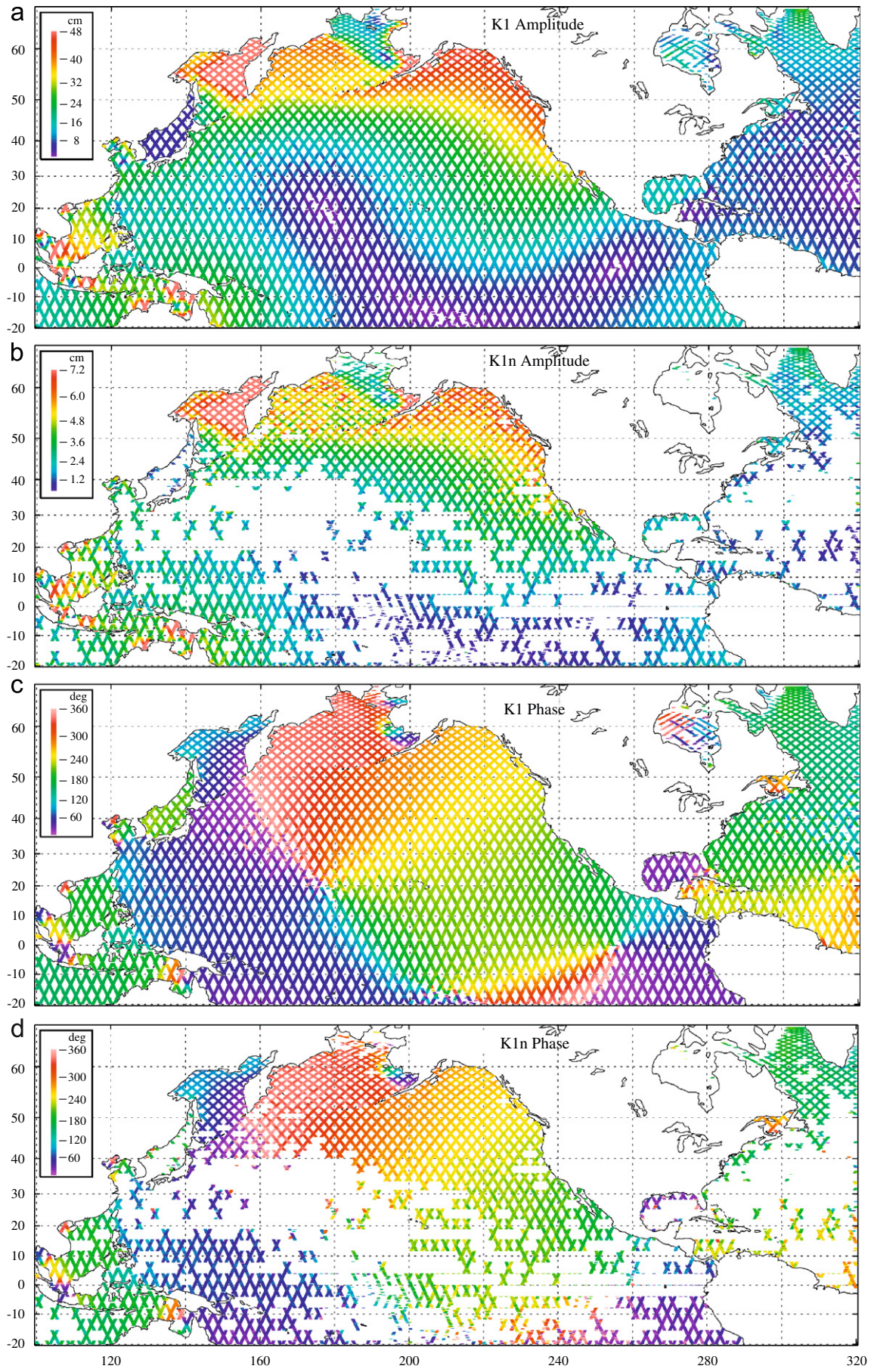

Fig. 3. Computed (a,b) amplitudes and (c,d) phases of (a,c) K_1 and (b,d) K_{1n}.

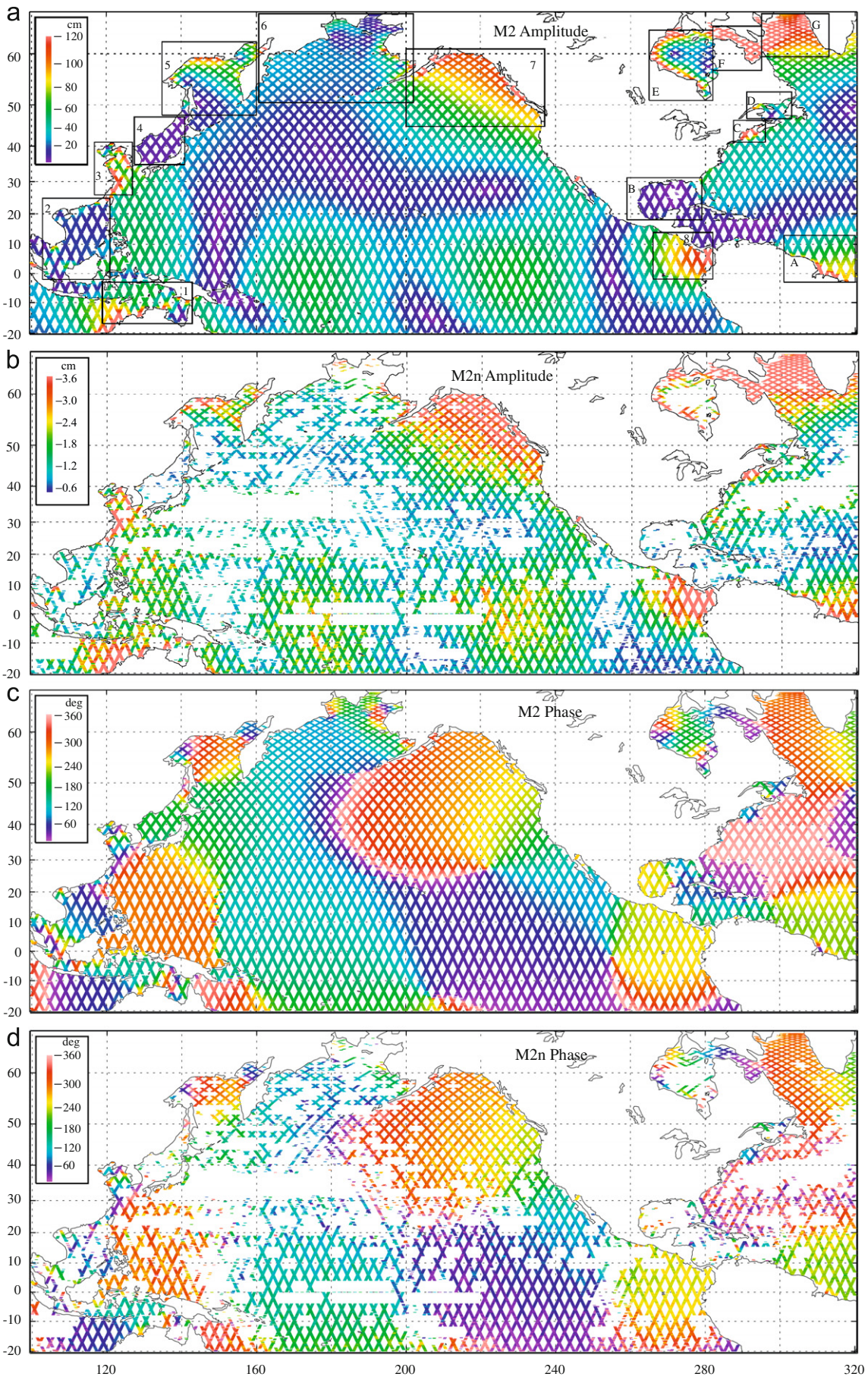

Fig. 4. Computed (a,b) amplitudes and (c,d) phases of (a,c) M_2 and (b,d) M_{2n}.

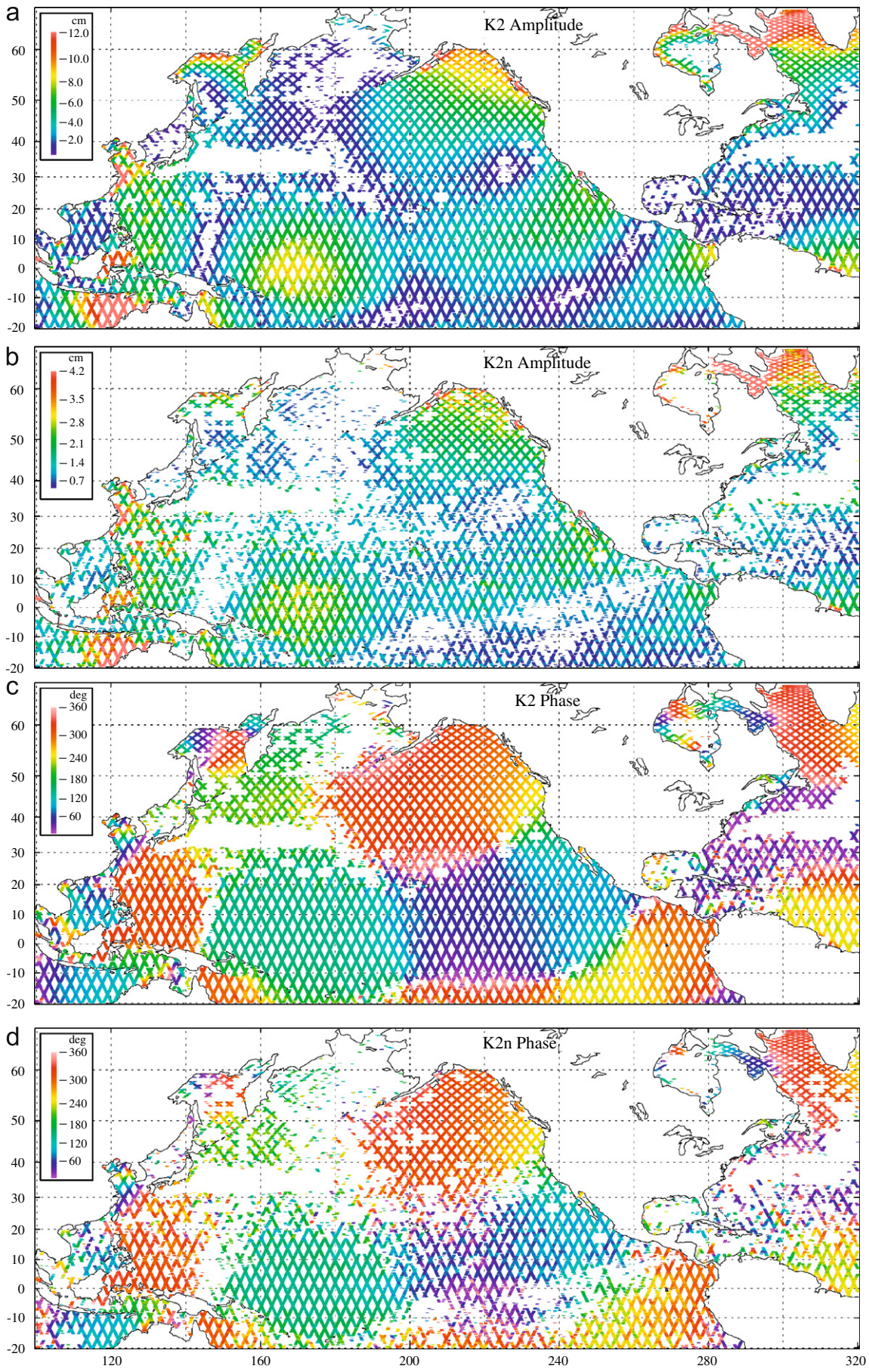

Fig. 5. Computed (a,b) amplitudes and (c,d) phases of (a,c) K_2 and (b,d) K_{2n}.

Table 2
Average amplitude ratios and phase differences (degrees) between nodal satellites and their parent constituents computed in each region (1–8 in the Pacific and A–G in the Atlantic) after applying the three editing criteria and excluding outliers outside two standard deviations.

Region	Q_{1n}/Q_1	O_{1n}/O_1	K_{1n}/K_1	M_{2n}/M_2	K_{2n}/K_2
Theory	0.1884	0.1885	0.1356	0.0373	0.2980
	0.0	0.0	0.0	0.0	0.0
Full	0.43 (0.34)	0.200 (0.038)	0.147 (0.034)	0.044 (0.015)	0.39 (0.20)
	−1.3 (38.3)	0.3 (12.1)	0.5 (12.9)	−0.6 (17.5)	1.1 (23.5)
1	0.260 (0.072)	0.190 (0.017)	0.138 (0.014)	0.0400 (0.0076)	0.308 (0.060)
	−5.0 (18.9)	−0.2 (6.3)	−0.5 (5.9)	−0.6 (11.0)	4.0 (16.5)
2	0.237 (0.067)	0.185 (0.015)	0.135 (0.018)		
	4.2 (22.3)	1.0 (5.4)	0.1 (7.7)		
3		0.191 (0.035)	0.139 (0.019)	0.0376 (0.0062)	0.330 (0.076)
		1.0 (8.8)	−0.8 (11.9)	1.3 (13.8)	−3.0 (11.2)
4		0.207 (0.043)			
		5.8 (17.7)			
5	0.222 (0.063)	0.194 (0.010)	0.147 (0.012)	0.043 (0.011)	0.39 (0.12)
	−3.3 (18.6)	−1.0 (5.2)	−0.7 (5.8)	−3.9 (16.3)	0.3 (22.5)
6	0.225 (0.052)	0.201 (0.040)	0.144 (0.021)	0.048 (0.014)	
	−4.3 (18.2)	−0.5 (7.7)	−0.9 (7.5)	−1.2 (19.0)	
7	0.231 (0.052)	0.190 (0.010)	0.139 (0.008)	0.0376 (0.0041)	0.314 (0.035)
	0.9 (15.4)	1.5 (3.4)	0.0 (3.2)	−0.1 (6.9)	0.3 (9.4)
8			0.157 (0.043)	0.0392 (0.0043)	0.259 (0.055)
			5.3 (14.5)	−0.3 (5.6)	−1.9 (14.1)
A		0.190 (0.039)	0.158 (0.033)	0.0379 (0.0044)	0.269 (0.061)
		−1.7 (10.8)	0.3 (18.4)	−0.9 (7.1)	−6.5 (15.6)
B		0.192 (0.040)	0.150 (0.051)		
		−0.6 (13.5)	3.1 (29.0)		
C		0.183 (0.041)	0.155 (0.031)	0.0351 (0.0038)	0.340 (0.077)
		10.6 (8.8)	−17.8 (14.8)	1.3 (5.9)	10.7 (20.5)
D		0.188 (0.027)	0.143 (0.029)	0.044 (0.012)	0.39 (0.16)
		−2.4 (7.2)	0.6 (9.3)	0.4 (9.5)	7.3 (27.2)
E				0.044 (0.012)	0.40 (0.12)
				−2.6 (16.4)	2.4 (15.6)
F		0.291 (0.050)	0.198 (0.057)	0.0363 (0.0028)	0.305 (0.023)
		−2.3 (13.7)	17.7 (12.9)	−1.0 (4.3)	−1.2 (4.8)
G		0.213 (0.035)	0.144 (0.026)	0.0402 (0.0039)	0.312 (0.038)
		−1.5 (10.3)	2.4 (9.2)	−2.6 (7.0)	0.8 (7.6)

Values in parentheses are the corresponding standard deviations.

4. Analysis results

Figs. 1–5 display the amplitudes and phases for five major constituents Q_1, O_1, K_1, M_2 and K_2 and their 18.6-year nodal satellites Q_{1n}, O_{1n}, K_{1n}, M_{2n} and K_{2n}. In areas not excluded by the above edit criteria, these figures show remarkable agreement in spatial patterns for each parent–satellite pair. This spatial agreement between the nodal satellites and their parents is as expected from their very close frequencies (separated by only $1/18.6\,\text{year}^{-1}$), which govern coastal and shelf wave response and propagation speeds.

Average amplitude ratios between each of these satellites and their parents are listed in Table 2 for the complete area shown in Figs. 1–5, as well as for 15 select regions, eight of them in Pacific Ocean (numbered 1–8 in Figs. 2 and 4) and seven in the western Atlantic Ocean (A–G). Some of the regions are dominated by diurnal tides, others by semidiurnals. Hence, the analysed amplitude ratios tend to be close to their theoretical values, but not everywhere. In general, they exceed these ratios due to likely contributions from aliased non-tidal signals, and more so for the weaker satellites. Phase values of nodal satellites also agree quite well with their parent constituents, even for the weaker satellites, such as M_{2n} (Fig. 4), though there are some differences, of the order of $\pm 10^{\circ}$.

Regional mean amplitudes of the four strongest constituents O_1, K_1, M_2 and K_2 and of their nodal satellites are summarized in Table 3 (see also Figs. 1, 2, 4 and 5). Instead of using the analysed amplitudes of nodal satellites, which are subject to contamination by noise and reduced number of observations (N_v), we computed their amplitudes using parent constituent amplitudes multiplied by the theoretical ratios (Table 2). The source of nodal variations in each region depends on whether diurnal or

Table 3
Average amplitudes (in cm) of diurnal O_1 and K_1 and semidiurnal M_2 and K_2 constituents in each region and their nodal satellite amplitudes from theoretical ratios (Table 2).

Region	O_1	O_{1n}	K_1	K_{1n}	M_2	M_{2n}	K_2	K_{2n}	
1	25.1	4.7	35.3	4.8	65.0	2.4	8.7	2.6	D
2	28.5	5.4	33.9	4.6	22.8	0.9	3.1	0.9	D
3	16.5	3.1	22.3	3.0	86.9	3.2	9.5	2.8	M
4	5.1	1.0	5.4	0.7	5.8	0.2	1.1	0.3	D
5	38.4	7.2	50.4	6.8	38.4	1.4	4.6	1.4	D
6	21.5	4.1	32.3	4.4	28.3	1.1	2.2	0.7	D
7	25.0	4.7	40.0	5.4	82.4	3.1	7.3	2.2	D
8	2.8	0.5	9.6	1.3	87.7	3.3	5.8	1.7	S
A	7.1	1.3	7.5	1.0	63.9	2.4	5.7	1.7	S
B	13.5	2.5	14.5	2.0	7.5	0.3	1.5	0.4	D
C	9.3	1.8	11.5	1.6	102.9	3.8	4.3	1.3	S
D	14.3	2.7	14.1	1.9	38.6	1.4	4.0	1.2	D
E	3.6	0.7	12.1	1.6	61.7	2.3	7.6	2.3	S
F	8.0	1.5	16.4	2.2	274.4	10.2	26.6	7.9	S
G	8.9	1.7	17.3	2.3	114.0	4.3	11.4	3.4	S

The corresponding *nodal character* of each region is marked in the last column, "D" for diurnal-dominant nodal variations, "S" for semidiurnal, or "M" for mixed.

semidiurnal tides are prevalent and on the nodal ratio of each constituent. In analogy with major constituents, we define a *nodal character* for each region, marked in Table 3 as "D" for diurnal-dominant nodal variations, "S" for semidiurnal and "M" for mixed nodal tides.

Six out of the eight regions in the Pacific Ocean are classified as *nodal diurnal*, with only the Gulf of Panama (region 8) exhibiting a *nodal semidiurnal* character. While M_2 is the dominant constituent in the Yellow and East China Seas (region 3), the relatively small nodal ratio (0.037) for M_{2n} and the fairly significant diurnal tides in this area cause this region to be classified as *nodal mixed*. Both the Sea of Okhotsk (region 5) and the Bering Sea (region 6) are dominated by diurnal tides and are therefore *nodal diurnal*. M_2 tides in the Gulf of Alaska are larger than either O_1 or K_1. However, this area (region 7) is still classified as predominantly *nodal diurnal*.

The situation is somewhat reversed in the western Atlantic Ocean, where semidiurnal tides dominate to such an extent that five of its seven listed regions are classified as *nodal semidiurnal*. Only the Gulf of Mexico (region B) is dominated by diurnal tides and is therefore *nodal diurnal*, while the Gulf of St. Lawrence (region D) is *nodal diurnal* for the same reasons as the Gulf of Alaska. The Northwest Atlantic Ocean has two areas which compete for the largest M_2 tides in the world. These are Bay of Fundy (in region C) and Ungava Bay (in region F), where M_2 amplitudes exceed 400 cm. It is therefore not surprising that these

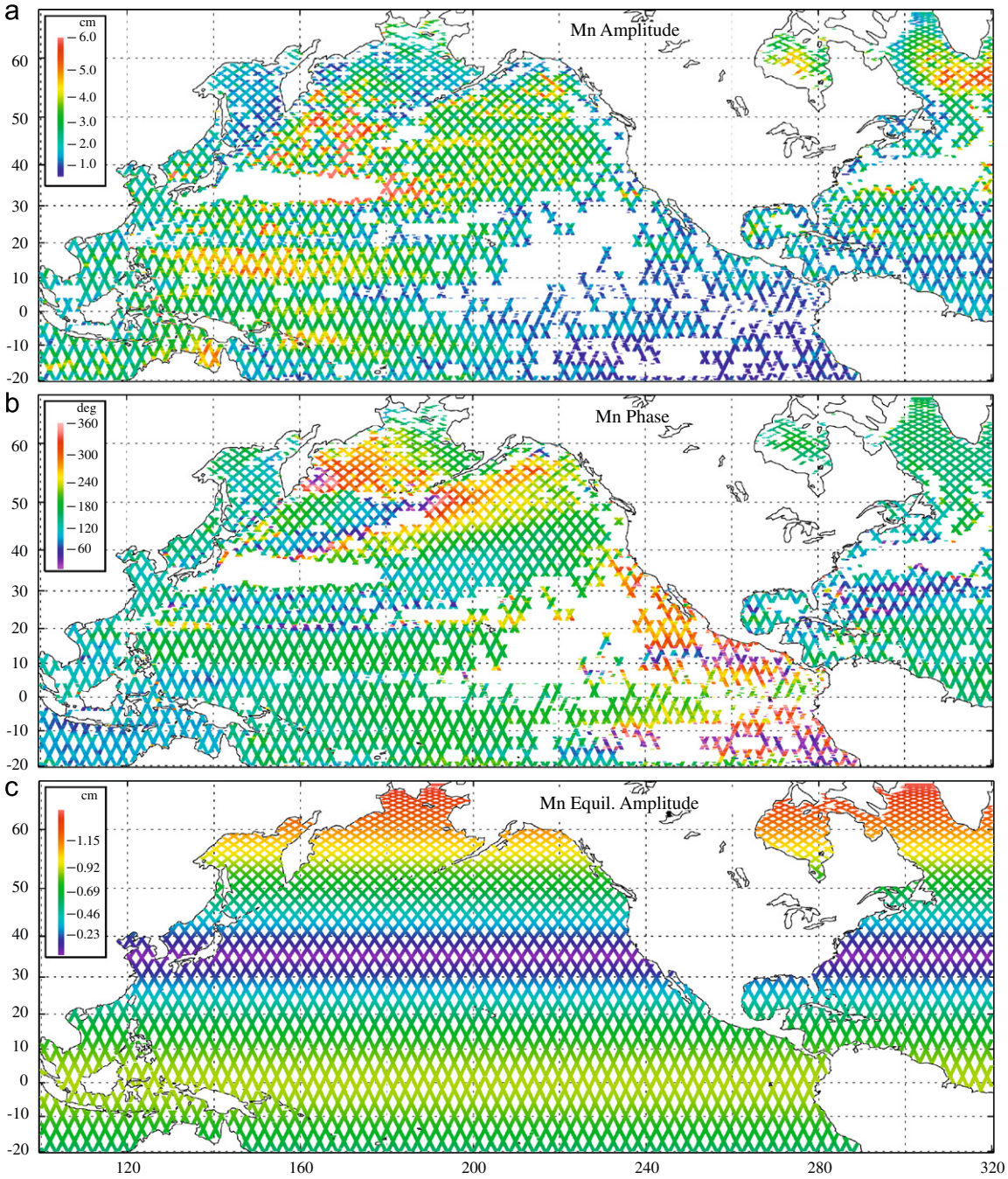

Fig. 6. Computed (a) amplitudes and (b) phases of M_n and (c) the equilibrium amplitude of M_n.

regions and the adjacent areas of Hudson Bay (region E) and northern Labrador Sea (region G) are predominantly *nodal semidiurnal*.

We also included in the analysis the 18.6-year constituent M_n. Its amplitudes (Fig. 6a) appear to be quite small, 1.5–3.5 cm over most of the area, and phase values (Fig. 6b) are clustered in the $163 \pm 64^{\circ}$ range. Even after applying our edit criteria, which eliminated most of the areas of the Kuroshio, the Oyashio, the Gulfstream and their extensions, there are clear anomalies in M_n amplitudes and phases in the areas of enhanced decadal variability and eddy activity, for example, east of the Korean Peninsula (cf. Kang et al., 2005) and in the Oyashio Current and its extension area. Because of its small amplitude and the effects of decadal ocean variability, such as the Pacific Decadal Oscillation, the altimetry-derived M_n amplitudes and phase values likely arise from this variability and not the nodal tide.

The theoretical 18.6-year nodal tide is a function of latitude, $0.9(3\sin^2\phi - 1)\cos N$ cm (e.g., Pugh, 1987), where N is the current longitude of the moon's ascending node. Its amplitude has a distinct zonal structure and is less than 1 cm almost everywhere (Fig. 6c). This is well below the level of natural ocean variability at this low frequency and the mean amplitude of the analysed M_n, which is about 2.5 cm (Table 1). Given the nonstationary nature of decadal ocean variability, our along track results for the M_n amplitudes from altimetry data covering less than one period do not contradict the results of Trupin and Wahr (1990), who were able to get a good fit to the theoretical 18.6-year spectral peak by "stacking" much longer time series of yearly averaged global data set of 260 coastal tide gauges.

5. Conclusions

In many parts of the ocean 16 years of collocated TPJ altimetry data are long enough for harmonic analyses to adequately separate the nodal satellites Q_{1n}, O_{1n}, K_{1n}, M_{2n} and K_{2n} from their parent constituents Q_1, O_1, K_1, M_2 and K_2, even for the weaker satellites Q_{1n}, M_{2n} and K_{2n}, with mean amplitudes between 1 and 2 cm. The utility of such analyses is evident from a relatively good agreement between the corresponding amplitude and phase patterns in Figs. 1–5 and from small off-diagonal elements in the error covariance matrices.

However, due to the relatively small amplitudes of these satellites (Table 1) and the likely influence from low-frequency aliased signals, the observed amplitude ratios between the nodal satellites and their parent constituents tend to exceed the values predicted from equilibrium tidal theory. This amplitude excess tends to be minimal where parent amplitudes are relatively large, for example, in the Sea of Okhotsk for diurnal and in the Yellow and East China Seas for semidiurnal constituents.

Examination of diurnal and semidiurnal nodal amplitudes in select coastal areas and marginal seas around the Pacific and the

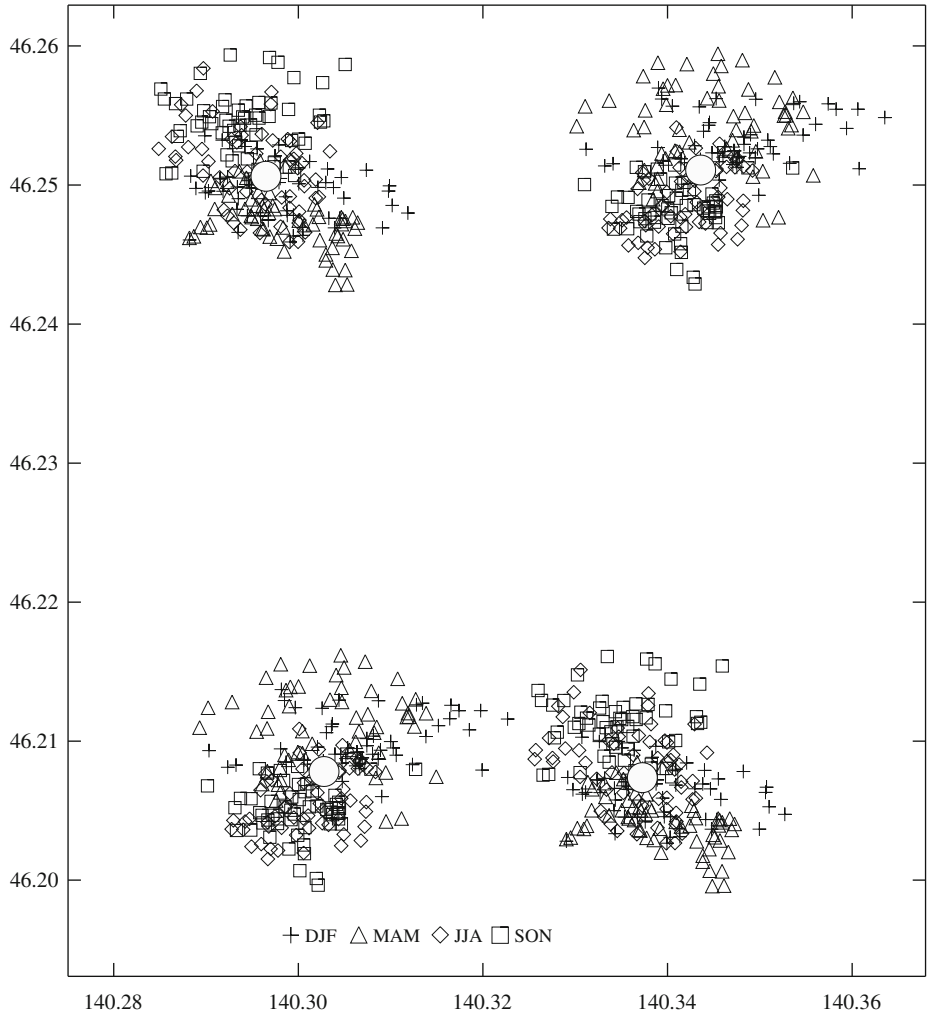

Fig. A1. Four data clusters near a crossover of Jason-1 passes 60 and 203 after along-track interpolation to 1-s time intervals. Four symbols show data locations during the months of winter (DJF), spring (MAM), summer (JJA) and fall (SON). Solid white circles mark mean "collocated" coordinates assigned to each data cluster.

western Atlantic Oceans allowed the assignment of a *nodal character* to these regions, which were classified as *nodal diurnal*, *nodal semidiurnal*, or *nodal mixed*, based on the nodal amplitudes in each band. While the areas with predominant diurnal tides are all *nodal diurnal*, due to their relatively large (0.19 and 0.14) nodal amplitude ratios, the small nodal ratio of 0.037 for M_{2n} resulted in some regions with strong M_2 tides to be classified as *nodal diurnal* or *nodal mixed*. The amplitude ratio between K_{2n} and K_2 is 0.30, making the K_{2n} amplitudes sometimes comparable to those of M_{2n}. However, this effect was not sufficient to make all of the areas with dominant M_2 to be dominant *nodal semidiurnal*.

The observed amplitudes of the 18.6-year constituent M_n are relatively small (Fig. 6). However, they significantly exceed theoretical nodal tide amplitudes at these latitudes. The analysed M_n are therefore of non-tidal origin, likely due to broad-band ocean variability with non-stationary phases at this $(18.6\,\text{year})^{-1}$ frequency.

Acknowledgements

We are grateful to Richard Ray for his discussion regarding nodal constituents and thank the two reviewers and the editor for their helpful comments and suggestions. This work was supported in part by the Korea Ocean Research and Development Institute (KORDI research program PG47100) and by Fisheries and Oceans Canada.

Appendix A. Collocation of along-track data

For each altimeter cycle and pass in the selected area, the along-track data were first filtered for small-scale noise by applying twice an along-track 3-point median filter. The filtered data were then interpolated to exact 1-s time intervals (ground track separation of about 5.8 km), counting from the equator crossing for ascending and to equator crossing for descending passes. Because of seasonal and longer-term variations in satellite orbits, these 1-s samples are actually spread over a small area, forming patches with nominal (rms) radii of the order of 1 km at mid-latitudes (Fig. A1). For the purposes of this study, we consider these patches to be sufficiently small and thus "collocated" in space.

Appendix B. Constituent error-covariance

CFCH discussed the use of error covariance matrices, computed from a least-squares solution of the overdetermined problem, for

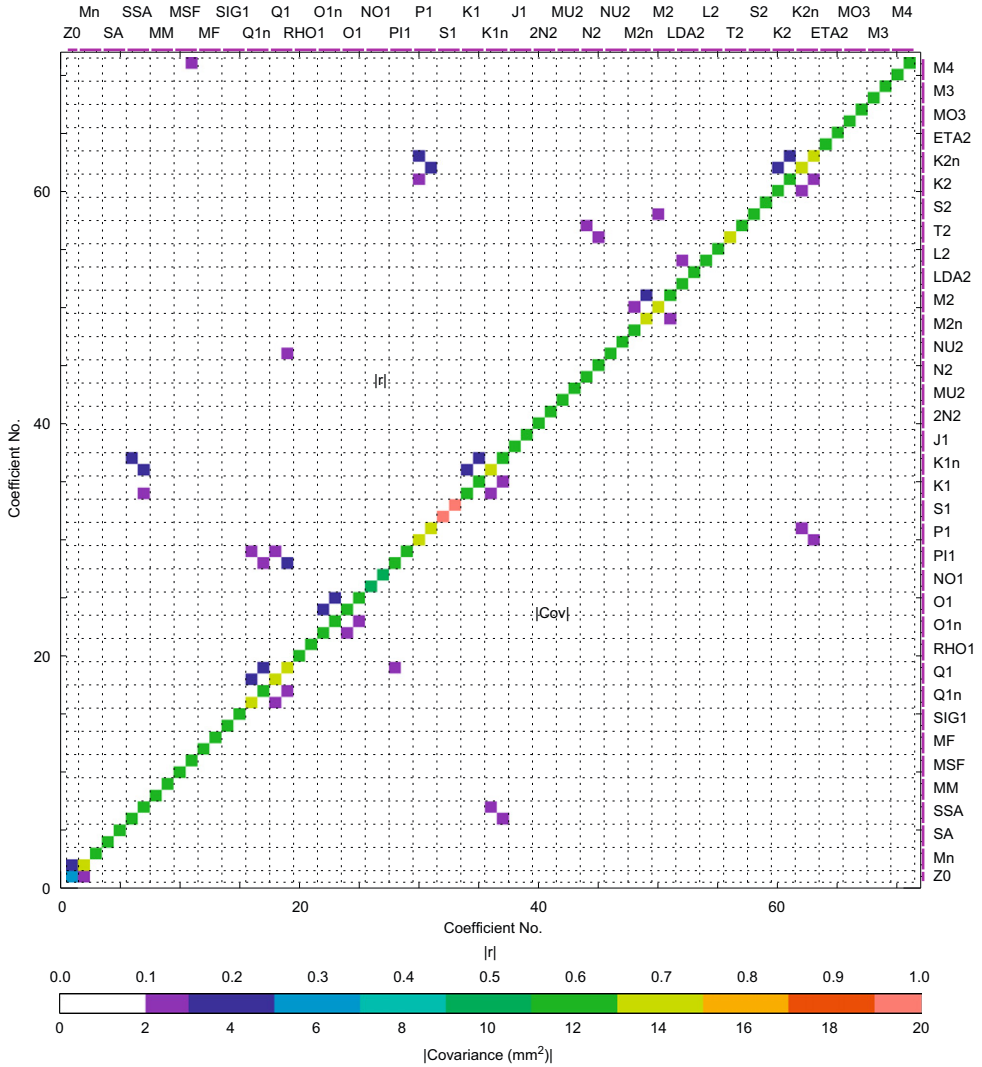

Fig. B1. An example of the error covariance matrix c_{ij} at an along-track location south of the Korean Peninsula (34.4N, 128.7E). As this matrix is symmetrical, $|c_{ij}|$ values are shown below and on the diagonal and correlation coefficients $|r_{ij}|$ above the diagonal.

Table B1
Aliased constituent pairs which require more than 3400 days to separate.

	$Q_1 : Q_{1n}$	$O_1 : O_{1n}$	$P_1 : K_2$	$P_1 : K_{2n}$	$K_1 : S_{sa}$	$K_1 : K_{1n}$	$K_{1n} : S_{sa}$	$M_2 : M_{2n}$	$K_2 : K_{2n}$
R	0.88	0.88	1.75	0.88	1.75	0.88	0.88	0.88	0.88
T_{min}	6798	6798	3404	6820	3404	6798	6798	6798	6796

R is the Rayleigh number and T_{min} (in days) is a minimum period required to resolve the two constituents, based on TPJ cycle period of 9.916 days and time series duration of 5970 days.

additional guidance on selection of tidal constituents and for assessment of aliasing and validity of local solutions. Fig. B1 shows an example of the error covariance matrix $c_{ij} = \mathrm{cov}(x_i, x_j)$, where x_i $(i = 1, \ldots, 2K-1)$ is the solution vector of sine and cosine coefficients. For $K = 36$ tidal constituents listed in Table 1, this matrix has 71×71 elements.

As this matrix is symmetrical, $|c_{ij}|$ values are shown in Fig. B1 below and on the diagonal, while correlation coefficients $|r_{ij}| = |c_{ij}|/(c_{ii}c_{jj})^{1/2}$ are shown above the diagonal. At this particular location (34.43N, 128.74E), the number of valid observations is $M = 538$ (out of possible 624) and the maximum error variance values on the diagonal are about 17 mm^2 for the two coefficients of S_1. In general, the error covariances are quite small for this 16.3-year long data set, compared to their values in CFCH, where $M < 250$.

For a tidal constituent k, an estimate of its amplitude error was defined in CFCH from their Eq. (6) as $\sigma_k = (c_{2k-2,2k-2} + c_{2k-1,2k-1})^{1/2}$ for $k = 2, \ldots, K$ and $\sigma_1 = c_{1,1}^{1/2}$ for Z_0. This was redefined here as $\sigma_k = (\sum_{i=1,2K-1}(c_{i,2k-2}^2 + c_{i,2k-1}^2)^{1/2})^{1/2}$, thus also including the off-diagonal elements, though over most of the area the off-diagonal terms are relatively small, with their combined contribution to σ_k usually less than 20%. Only a few off-diagonal $|c_{ij}|$ in Fig. B1 approach 3−4 mm^2, for example, $P_1 - K_{2n}$ and $S_{sa} - K_{1n}$.

The $|r_{ij}|$ values in this figure are somewhat larger between the 18.6-year satellites and their parent constituents, as well as for $S_{sa} - K_{1n}$, $P_1 - K_{2n}$ and $Z_0 - M_n$ pairs. This is as expected, as for these pairs the Rayleigh criterion is $R < 1$, for a TPJ time series with a duration of approximately 5970 days, while the minimum period T_{min} required to resolve all the nodal constituents is about 6800 days (Table B1).

References

Amin, M., 1985. Temporal variations of tides on the west coast of Great Britain. Geophys. J. R. Astr. Soc. 82, 279–299.

Amin, M., 1993. Changing mean sea level and tidal constants on the west coast of Australia. Aust. J. Mar. Freshwater Res. 44, 911–925.

Cherniawsky, J.Y., Foreman, M.G.G., Crawford, W.R., Henry, R.F., 2001. Ocean tides from TOPEX/POSEIDON sea level data. J. Atmos. Oceanic Technol. 18, 649–664.

Doodson, A.T., 1921. The harmonic development of the tide-generating potential. Proc. R. Soc. (London) Ser. A 100, 306–323.

Doodson, A.T., 1924. Perturbations of harmonic tidal constants. Proc. R. Soc. (London) Ser. A 106, 513–526.

Egbert, G.D., Bennett, A.F., Foreman, M.G.G., 1994. TOPEX/POSEIDON tides estimated using a global inverse model. J. Geophys. Res. 99, 24821–24852.

Egbert, G.D., Erofeeva, S.Y., 2002. Efficient inverse modelling of barotropic ocean tides. J. Atmos. Oceanic Technol. 19, 183–204.

Foreman, M.G.G., 1977. Manual for tidal heights analysis and prediction. Pacific Marine Science Report No. 77–10, Institute of Ocean Sciences, Patricia Bay, Sidney, B.C., 66pp.

Foreman, M.G.G., Neufeld, E.T., 1991. Harmonic tidal analyses of long time series. Int. Hydrogr. Rev. LXVIII (1), 85–109.

Foreman, M.G.G., Crawford, W.R., Cherniawsky, J.Y., Henry, R.F., Tarbotton, M.R., 2000. A high-resolution assimilating tidal model for the northeast Pacific Ocean. J. Geophys. Res. 105, 28629–28651.

Foreman, M.G.G., Cummins, P.F., Cherniawsky, J.Y., Stabeno, P., 2006. Tidal energy in the Bering Sea. J. Mar. Res. 64, 797–818.

Garrett, C., 1979. Mixing in the ocean interior. Dyn. Atmos. Ocean 3, 239–265.

Godin, G., 1972. The Analysis of Tides. University of Toronto Press, Toronto, Ontario 264pp.

Godin, G., 1986. The use of nodal corrections in the calculation of harmonic constants. Int. Hydrogr. Rev. LXIII (2), 143–162.

Hasumi, H., Yasuda, I., Tatebe, H., Kimoto, M., 2008. Pacific bidecadal climate variability regulated by tidal mixing around the Kuril Islands. Geophys. Res. Lett. 35, L14601 10.1029/2008GL034406.

Kang, S.K., Cherniawsky, J.Y., Foreman, M.G.G., Min, H.S., Kim, C.-H., Kang, H.-W., 2005. Patterns of recent sea level rise in the East/Japan Sea from satellite altimetry and in situ data. J. Geophys. Res. 110, C07002 10.1029/2004JC002565.

Kaye, C.A., Stuckey, G.W., 1973. Nodal tidal cycle of 18.6 yr: its importance in sea-level curves of the east coast of the United States and its value in explaining long-term sea-level changes. Geology 1, 141–144.

Ku, L.-F., Greenberg, D.A., Garrett, C.J.R., Dobson, F.W., 1985. Nodal modulation of the lunar semidiurnal tide in the Bay of Fundy and Gulf of Maine. Science 230, 69–71.

Le Provost, C., Lyard, F., Molines, J.M., Genco, M.L., Rabilloud, F., 1998. A hydrodynamic ocean tide model improved by assimilating a satellite altimeter-derived data set. J. Geophys. Res. 103, 5513–5529.

Loder, J.W., Garrett, C.J.R., 1978. The 18.6-year cycle of sea surface temperature in shallow seas due to variations in tidal mixing. J. Geophys. Res. 83, 1967–1970.

McKinnell, S.M., Crawford, W.R., 2007. The 18.6-year lunar nodal cycle and surface temperature variability in the northwest Pacific. J. Geophys. Res. 112, C02002 10.1029/2006JC003671.

Munk, W.H., Cartwright, D.E., 1966. Tidal spectroscopy and prediction. Phil. Trans. R. Soc. London 259A, 533–581.

Munk, W.H., Dzieciuch, M., Jayne, S., 2002. Millenial climate variability: is there a tidal connection? J. Clim. 15, 370–385.

Naeije, M., Doornbos, E., Mathers, L., Scharroo, R., Schrama, E., Visser, P., 2002. Radar Altimeter Database System: Exploitation and extension (RADSxx). Final Report. NUSP-2 report 02-06, NUSP-2 project 6.3/IS-66. Space Research Organisation Netherlands (SRON), Utrecht, The Netherlands, 99+xiiipp.

Osafune, S., Yasuda, I., 2006. Bidecadal variability in the intermediate waters of the northwestern subarctic Pacific and Okhotsk Sea in relation to 18.6-year period nodal cycle. J. Geophys. Res. 111, C05007 10.1029/2005JC003277.

Parke, M.E., Stewart, R.H., Farless, D.L., Cartwright, D.E., 1987. On the choice of orbits for an altimetric satellite to study ocean circulation and tides. J. Geophys. Res. 92, 11693–11707.

Parker, K.S., Royer, T.C., Deriso, R.B., 1995. High-latitude climate forcing and tidal mixing by the 18.6-year lunar nodal cycle and low-frequency recruitment trends in Pacific halibut (*Hippoglossus stenolepis*). In: Beamish, R.J. (Ed.), Climate change and northern fish populations. Can. Spec. Publ. Fish. Aquat. Sci. 121, pp. 447–459.

Pugh, D.T., 1987. Tides, Surges, and Mean Sea Level. Wiley, New York 472pp.

Ray, R.D., 1998. Spectral analysis of highly aliased sea-level signals. J. Geophys. Res. 103, 24991–25003.

Ray, R.D., 1999. A global ocean tide model from TOPEX/Poseidon altimetry: GOT99. NASA Technical Memorandum 209478, Goddard Space Flight Center, 55pp.

Ray, R.D., 2007. Decadal climate variability: is there a tidal connection? J. Clim. 20, 3542–3560.

Royer, T.C., 1993. High-latitude oceanic variability associated with the 18.6-year nodal tide. J. Geophys. Res. 98, 4639–4644.

Scharroo, R., 2008. RADS Version 3.0 User Manual and Format Specification. Delft University of Technology, The Netherlands 51pp.

Schrama, E.J.O., Ray, R.D., 1994. A preliminary tidal analysis of TOPEX/POSEIDON altimetry. J. Geophys. Res. 199, 24799–24808.

Schrama E.J.O., Scharroo, R., Naeije, M., 2000. Radar Altimeter Database System (RADS): Towards a generic multi-satellite altimeter database system. USP-2 Report 00-11, BCRS/SRON, Delft, The Netherlands, ISBN 90-54-11-319-7, 88pp.

Trupin, A., Wahr, J., 1990. Spectroscopic analysis of global tide gauge sea level data. Geophys. J. Int. 100, 441–453.

Yasuda, I., Osafune, S., Tatebe, H., 2006. Possible explanation linking 18.6-year period nodal cycle with bi-decadal variations of ocean and climate in the North Pacific. Geophys. Res. Lett. 33, L08606 10.1029/205GL025237.

Yndestad, H., 2006. The influence of the lunar nodal cycle on Arctic climate. J. Mar. Sci. 63, 401–420.

Yndestad, H., Turrell, W.R., Ozhigin, V., 2008. Lunar nodal tide effects on variability of sea level, temperature and salinity in the Faeroe-Shetland Channel and the Barents Sea. Deep-Sea Res. I 55, 1201–1217.